Hindawi
Scientific Programming
Volume 2022, Article ID 3119471, 8 pages
https://doi.org/10.1155/2022/3119471

Research Article

Cone-Beam Computed Tomography Image Features under Intelligent Three-Dimensional Reconstruction Algorithm in the Evaluation of Intraoperative and Postoperative Curative Effect of Dental Pulp Disease Using Root Canal Therapy

Lu Zhao, Jiaxin Pan, and Lingling Xu

Department of Stomatology, Affiliated Third Hospital of Soochow University, The First People's Hospital of Changzhou City, Changzhou 213003, Jiangsu, China

Correspondence should be addressed to Lu Zhao; zhaolu0106@czfph.com

Received 18 October 2021; Revised 9 January 2022; Accepted 12 January 2022; Published 2 February 2022

Academic Editor: M Pallikonda Rajasekaran

Objective. The objective of this study was to analyze the application effect of algorithm-based three-dimensional reconstruction of cone-beam computed tomography (CBCT) images in the treatment of dental pulp disease (DPD) and the evaluation of the curative effect after treatment. *Methods*. 120 patients with DPD in hospital were selected as the research objects. In this study, based on the regridding model in the algorithm, the mapping relationship between the undersampled CBCT image and the fully sampled CBCT image was connected, and a model that can be used for image restoration and reconstruction was obtained after training. The algorithm model was used to reconstruct and repair the CBCT images of the research objects, and then, the reconstructed CBCT images were segmented based on the improved level set algorithm. After that, it analyzed and compared the accuracy of X-ray and CBCT based on three-dimensional reconstruction for the diagnosis accuracy of DPD and compared the average bone density of patients and the effect of root canal filling in each time period after root canal treatment. *Result*. After the image was reconstructed with the regridding model, a CBCT image of the patient's teeth with less noise and clearer structure was obtained. The segmentation accuracy of the level set algorithm reached 85.5% on average, and the undersegmentation rate (UR) and the over-segmentation rate (OR) were both less than 6%. The diagnostic rates of X-ray and three-dimensional CBCT examination of DPD were 43.7% and 100%, respectively, and the difference was statistically significant ($P < 0.05$). Under the monitoring of the three-dimensional reconstruction of CBCT technology, the average bone density of the test group patients after 12 months of root canal treatment was the same as that of healthy people. Under X-ray examination, the average bone density of the test group patients was still lower than that of healthy people after 12 months of root canal treatment. Under the three-dimensional reconstruction of CBCT, the underfilling rate of patients after root canal treatment was 5%, the proper filling rate was 85%, and the overfilling rate was 10%. *Conclusion*. In summary, the CBCT reconstructed by the intelligent three-dimensional algorithm was effectively improved, which enhanced the image quality and segmentation efficiency. Analysis on diagnosis efficiency and treatment effect proved that CBCT can be an effective method to evaluate the initial curative effect of DPD treatment during and after the surgery and can provide valuable information in future dental treatment, thereby enhancing the success rate of DPD using root canal therapy.

1. Introduction

Diseases on the hard tissues of teeth are collectively called dental diseases, and dental diseases in a broad sense also include pulp diseases. Therefore, it can also be called dental pulp disease (DPD) [1]. Dental pulp tissue is the most important tissue in maintaining tooth nutrition, innervation, and immune function [2, 3]. Root canal therapy is the most commonly used effective treatment method for pulp disease and periapical disease in the world. The principle of root canal therapy is to remove most of the infections in the root canal through mechanical and chemical methods and to fill the root canal and seal the crown to prevent the occurrence of periapical lesions or promote the healing of existing periapical lesions [4, 5]. Although root canal therapy shows a good effect, it still fails in some cases. Early clinical treatment failure (within a few days or weeks) is affected by a variety of factors, which may be related to an incorrect diagnosis of pulp diseases. Moreover, poor assessment of pulp status may lead to a clinically severe underestimation of the severity of pulp inflammation. This negligence may lead to irreversible pulp inflammation and pulp tissue necrosis, leading to spontaneous and persistent pain after treatment. Therefore, the correct assessment of DPD and the selection of appropriate materials before targeted treatment are the keys to improving the prognostic effect and success rate of patients [6, 7].

In this regard, CBCT technology can provide high-precision three-dimensional images for dental treatment. As the name implies, it is a cone-beam projection computer recombination tomographic imaging device. Its principle is that the X-ray generator uses a low radiation dose (usually, the tube current is about 10 mA) to make a circular digital projection around the projection body. Then, the data obtained in the "intersection" after the digital projection are "reorganized" in the computer to obtain a three-dimensional image [8]. The projection principle of cone-beam computed tomography (CBCT) acquisition of data is completely different from traditional sector scan CT, and the algorithm principle of later computer reorganization is similar. CBCT was first used in dentistry in Europe in 1998 and was approved for use in the United States in 2001. In 2002, at the "twenty-first Century Craniofacial Imaging" seminar held in Pacific Grove, California, the early evaluation of the possible future impact of this technology on dentistry, especially orthodontics, was discussed for the first time [9, 10]. Since this seminar, CBCT technology has undergone rapid evolution, which is mainly due to the urgent need for accurate, reproducible, and safe three-dimensional images in various fields. In orthodontics, three-dimensional imaging can help unravel the complexities of dentistry and skeletal matrices and improve diagnosis and treatment planning for specific case types. Although CBCT technology has so many advantages, it also has some shortcomings, which hinder its extensive clinical development and application. For example, due to equipment and operation problems, it has strong noise and artifacts, resulting in poor image quality and unable to respond to lesion details. The intelligent three-dimensional reconstruction algorithm that has emerged in the past few years can compensate for the shortcomings well. Many related studies have shown that the intelligent three-dimensional reconstruction algorithm can well remove the noise and artifacts in the medical image, and the segmentation accuracy of the lesion is also high. Therefore, it is a popular algorithm in the field of medical image processing.

In this study, the three-dimensional reconstruction algorithm was used to reconstruct the CBCT images of DPD patients, and on this basis, the diagnosis and root canal treatment of DPD patients were carried out. In addition, it was compared with the diagnosis and treatment effect under X-ray detection. This study was expected to provide new ideas and reference basis for the diagnosis and treatment of clinically related diseases.

2. Methods

2.1. Research Objects. 120 patients who were about to undergo dental replacement surgery in the hospital were selected as the research objects, and 120 healthy people were selected in the control group. The average age was 48.1 ± 2.6 years. Routine oral clinical examinations were performed on the selected 120 patients. All patients were examined by CBCT and X-ray and had complete clinical diagnosis records and imaging data. Among the 120 patients, 80 were male patients and 40 were female patients. Finally, the inspection results were compared and analyzed.

The inclusion criteria were defined as follows: all patients were diagnosed with DPD in this hospital, and all had relevant radiological examination imaging data; the patients were in good physical condition and had no other major diseases in the body before treatment; patients whose teeth were maintained at natural dentition, and there was no congenital dental disease; and patients without disorder in the chewing system.

The exclusion criteria were given as follows: the patient's dental pulp had not been diagnosed in hospital, and the imaging data were incomplete; patients with other major diseases in the body; patients whose oral hygiene status was not up to standard; and patients with a history of related orthodontics or had previous maxillofacial surgery.

All patients had signed the informed consent forms. The research conducted in this study had been approved by the ethics committee of the hospital.

2.2. Research Methods. The same researcher performed traditional X-ray examinations and CBCT examinations on the teeth of 120 patients. Traditional X-ray examinations included traditional dental film and curved tomography; CBCT machine and digital dental medicine research software were used. The software can accept the DICOM file transmitted by the CT machine and perform the three-dimensional reconstruction. It can also measure the distance and angle of the image. CBCT scanned the patient's oral tissue, with the tube voltage of 90 kV, tube current of 5 mA, and scan time of 17.5 s. After rotation for 360°, it could continue scanning, reconstruct the original data image, and obtain three-dimensional images, including axial, sagittal, and coronal images. All images were displayed on a 24-inch LCD monitor with $1600 \times 1\ 200$ pixels and stored on the same computer. The images obtained from the inspection were compared and performed with the statistical analysis.

2.3. Three-Dimensional Reconstruction Algorithm. Because the data collected in the spatial frequency domain was distributed at unequal intervals, the image cannot be quickly reconstructed by Fourier transform, so the collected CT image data need to be gridded before the image can be reconstructed. An algorithm that is widely recognized and used in the algorithm is called the Jackson gridding algorithm [11], which is often used because of its simple calculation and less computing time. The calculation equation of this gridding algorithm was as follows:

$$F_n(\phi, v) = \{[F(\phi, v)k \times Tn(\phi, v)] * C(\phi, v)\} \times n(\varphi, v),$$
$$T_n(\phi, v) = \frac{T(\phi, v)}{T(\phi, v) * C(\phi, v)}. \tag{1}$$

In the above equation, F_n represented the CT image data for resampling, F represented the CT image data sampled without interval, T_n referred to the density compensation function of uneven sampling, C was the convolution function, n was the sampling function at equal intervals, and T referred to the sampling function at unequal intervals. In addition, $\times$ stood for multiplication, and $*$ referred to the convolution operation.

The function used in the Jackson gridding algorithm was the Kaiser–Bessel function, which was expressed as

$$s(\phi) = \frac{do(\alpha\sqrt{1-(2\phi/E)}\,\grave{\mathrm{U}}2)}{d_0(\alpha)}, |\phi|E\frac{E}{2}, \tag{2}$$

$$s(\phi) = 0,\ |\varphi|E\frac{E}{2}. \tag{3}$$

In equations (2) and (3), $s(\varphi)$ represented the Kaiser–Bessel function, d_o represented the zero-order deformed Bessel function, and E represented the window length.

The calculation expression of the CT image after the optimization and reconstruction of the grid algorithm was expressed as follows:

$$h_m(x, y) = h_n(x, y) \cdot \frac{p(x, y)}{c(x, y)}, \tag{4}$$

where h_m was the image reconstructed by the algorithm, h_n represented the Fourier transform of F_n, c referred to the inverse Fourier transform, and p represented the rectangular function.

With the further research and innovation of the gridding algorithm, people have improved the gridding algorithm to a certain extent and named the optimized gridding algorithm as the regridding algorithm [12], which was applied to the reconstruction of CT images. The expression of the regridding algorithm at this time was as follows:

$$Mr = \phi, \tag{5}$$

where M represented the sine interpolation coefficient matrix, r represented the n vector on the spatial data point on the grid, and φ referred to the m vector on the spatial data point on any trajectory. Because the calculation was too large, the word was selected to iteratively solve the approximate value of the equation:

$$\hat{r} = M * D\phi\ . \tag{6}$$

In equation (6), $\hat{\mathrm{r}}$ represented the approximate solution of r, $*$ was the Hermitian transpose, $D = \mathrm{diag}\ (d)$ represented the diagonal matrix, and d was the density-weighted m-dimensional vector. The following equation can be obtained by combining equations (5) and (6):

$$\hat{r} = M * DMr. \tag{7}$$

When the value of $M * D$ was infinitely close to M, d was the optimal solution at this moment. At this time, the calculation expression of d was given as follows:

$$d = diag\left(\theta\begin{bmatrix} f_k & 0 \\ 0 & 0 \end{bmatrix}\theta^*\right). \tag{8}$$

The matrix M can be replaced with the following calculation as soon as possible:

$$\mathrm{M} = \mathrm{TRUR}\, *. \tag{9}$$

In the above equation, T represented the Kaiser–Bessel interpolation matrix, R represented the Fourier matrix, U represented the diagonal matrix, and RUR^* represented the deconvolution result. Then, the below equation could be obtained by combining equations (5) and (9):

$$\mathrm{TRUR} * r = \phi,$$
$$\hat{r} = \mathrm{TRU} * R * D\phi. \tag{10}$$

Since the value of d_o of this method would be affected by the interpolation function, after research and further improvement, people use the iterative calculation method to optimize this method and improve the initial estimation of d_o, and the accurate valuation was calculated gradually starting from $d = d_o$:

$$d = \frac{d}{HH * d}. \tag{11}$$

The closer the HH $*$ d was to 1, the better the result of density weighting.

The undersampled CT image was reconstructed through the final regridding image reconstruction algorithm, and the equation was expressed as follows:

$$\mathrm{CT}_{\mathrm{highquality}} = \mathrm{F}\left(\mathrm{CT}_{\mathrm{lowquality}}\right). \tag{12}$$

In the equation above, $\mathrm{CT}_{\mathrm{lowquality}}$ represented the reconstructed CT image of undersampled spatial data, which contained a lot of noise and blur; $\mathrm{CT}_{\mathrm{highquality}}$ represented the reconstructed full-sampling CT image, and F represented the function learned by a convolutional neural network (CNN).

In this study, a CNN model was used to process the undersampled image, and finally, a fully sampled CT image was obtained. The calculation equation and structure are shown in Figure 1.

$$y_0 = y_i + T_3 * BM\left(\mathrm{Re}LU\left(T_2 * BM\left(\mathrm{Re}LU\left(T_1 * y_i + a_1\right)\right) + a_2\right)\right) + a_3. \tag{13}$$

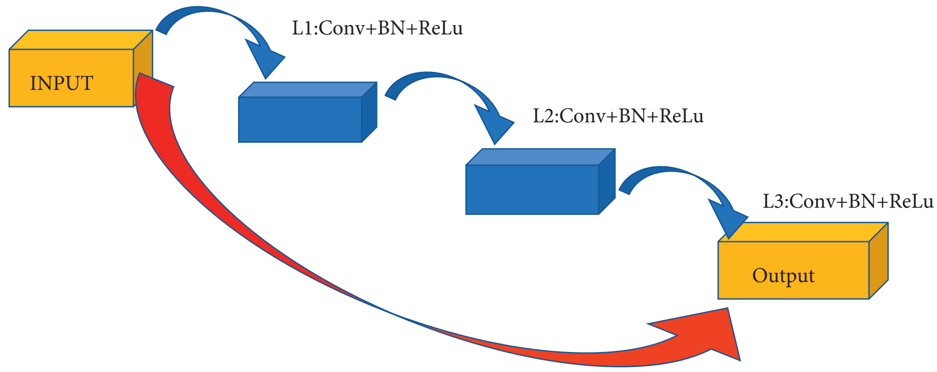

FIGURE 1: Schematic diagram of CNN structure.

In the equation (13) above, y_i represented the undersampled CT image; T_1, T_2, and T_3 represented the weight; a_1, a_2, and a_3 represented the offset; $*$ was the convolution operation, *ReLU* represented the activation function, and *BM* represented the regularization operation.

The loss function of the network model was expressed as follows:

$$f(Y, Z) = \frac{1}{N} * \sum_{j=1}^{N} \left| Y_j - Z_j \right|. \qquad (14)$$

In equation (14), Y_j was the pixel in the undersampled image, Z_j represented the pixel in the fully sampled image, N represented the number of pixels in the CT image, and $f(Y, Z)$ represented the loss function.

2.4. Statistical Mathematical Processing. The SPSS19.0 software was adopted for statistical analysis, the measurement data conforming to the normal distribution were represented by the mean ± standard deviation, and the comparison of differences among groups was analyzed by independent sample t-test. The measurement data that did not conform to the normal distribution were represented by the median value and the four-point position, and the comparison of differences among groups was analyzed by the nonparametric rank-sum test. Enumeration data were expressed by n (%), and the comparison of differences among groups was analyzed by chi-square test. The P value was calculated based on the variance value, and $P < 0.05$ meant the difference was statistically significant.

3. Results

3.1. CBCT Image Display Based on Intelligent Three-Dimensional Reconstruction Algorithm. The intelligent three-dimensional reconstruction algorithm was adopted to reconstruct and optimize the CBCT undersampled image of the selected patient's teeth, to obtain a fully sampled CBCT image of the patient's teeth that restored noise and blur. Comparative experimental results shown in Figure 2 revealed that the undersampled CBCT images of human teeth contained more noise and blur, and some structural images were obviously blurry. After the image was reconstructed with the regridding model, a CBCT image of the patient's teeth with less noise and clearer structure is obtained.

3.2. The Effect of Intelligent Three-Dimensional Reconstruction Algorithm on CBCT Image Processing. Figure 3 shows the quantitative evaluation results of the intelligent three-dimensional reconstruction algorithm on the CBCT image processing effect. It suggested that the segmentation accuracy of the intelligent three-dimensional reconstruction algorithm was greater than 85.5%, and the UR and OR were all less than 6%. Compared with the adaptive local threshold method, the average segmentation accuracy of the improved intelligent three-dimensional reconstruction algorithm was 84.7%, with an increase of 5.5%; the UR was averaged 5.3%, with a decrease of 5.7%; and the OR averaged 3.1%, with an increase of 1.1%. The results before and after segmentation were shown in Figure 3.

3.3. The Accuracy of CBCT in the Diagnosis of DPD. After hip replacement for the subjects, the postoperative complications of the subjects were diagnosed through three-dimensional CT and X-ray. The X-ray and CT images of patients were submitted to the experienced radiologists for analysis and observation, and the diagnostic effects of X-ray and three-dimensional CT diagnosis of postoperative complications were analyzed. The DPD diagnostic rates of X-ray and three-dimensional CBCT examination were 43.7% and 100%, respectively, and the difference was statistically significant ($P < 0.05$). The specific details are shown in Figure 4.

3.4. CBCT Analysis of Treatment Effect after DPD Treatment. In this study, the patients participating in the study underwent a complete root canal therapy, and the average bone density around the apex of the teeth after root canal therapy was detected through the three-dimensional reconstructed CBCT images. In addition, the average bone mineral density of the patient during the 12 months after treatment was examined by X-ray, and the analysis of the treatment effect of the patient's root canal therapy by the two imaging methods was compared. Compared with the healthy teeth of the control group, under the CBCT examination, the average

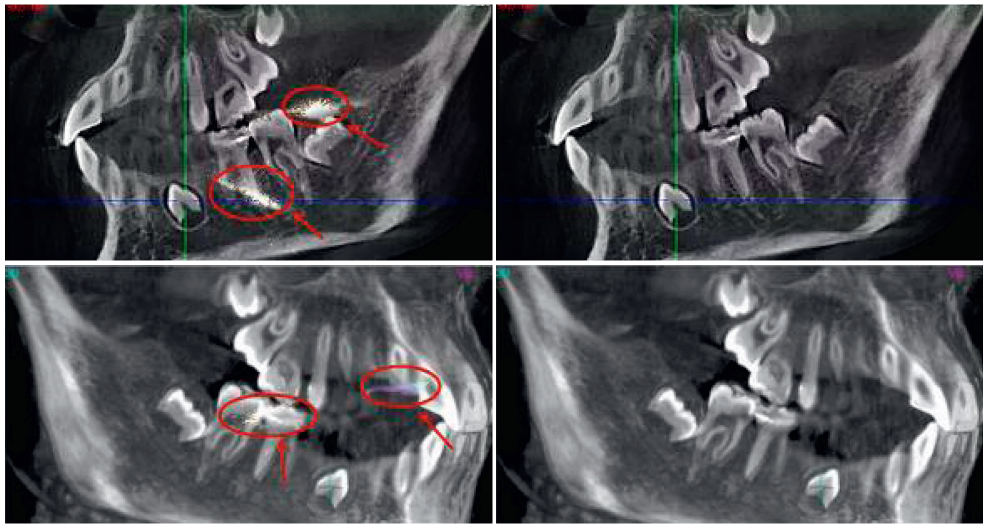

Figure 2: CBCT images reconstructed using the regridding algorithm. Note: the part circled in red referred to the diseased part of the patient's teeth.

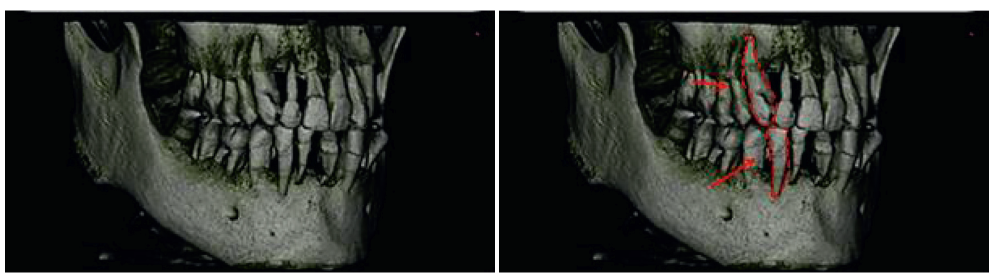

Figure 3: Comparison of the segmentation results of patients' teeth based on three-dimensional reconstruction algorithms.

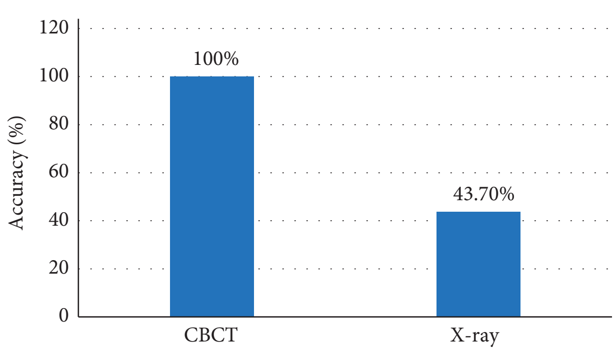

Figure 4: DPD diagnostic rates of X-ray and three-dimensional CBCT examinations.

bone density of the teeth of the control group after root canal therapy continued to increase 3 months, 9 months, and 12 months after the surgery and finally had the same bone density with the healthy teeth. After comparison on the data between the two groups, it was found that the P value was less than 0.05, so there was a statistically significant difference, as shown in Figures 5 and 6.

3.5. Comparison of the Filling Effect of Root Canal Therapy in DPD. In addition to the analysis of bone density, the effect of root canal filling in patients after root canal therapy was analyzed in this study. Based on the three-dimensional reconstructed CBCT image (as shown in Figure 7), the underfilling rate of the patient's root canal therapy was 6 (5%), the proper filling rate was 102 (85%), and the over-filling rate was 12 (10%).

4. Discussion

DPD is a disease that occurs in the hard tissues of the tooth, such as tooth decay. Destructive diseases of dental hard tissues caused by bacterial infection, or necrosis of dental pulp tissue caused by dental nerves, belong to the scope of treatment of DPD and also include noncarious diseases, such as wedge-shaped defects caused by horizontal brushing. Caries refers to damage to the hard tissue of the teeth caused by the combined action of multiple factors in the oral cavity, which is manifested by the demineralization of inorganic matter and the decomposition of organic matter. As the course of the disease progresses, there is an evolution process from color change to substantial lesions, and it is characterized by high incidence and wide distribution. Generally, the average prevalence of dental caries can be around 50% [13, 14]. It is the main common disease in the oral cavity and one of the most common diseases in humans. The WHO has listed it alongside cancer and cardiovascular disease as the

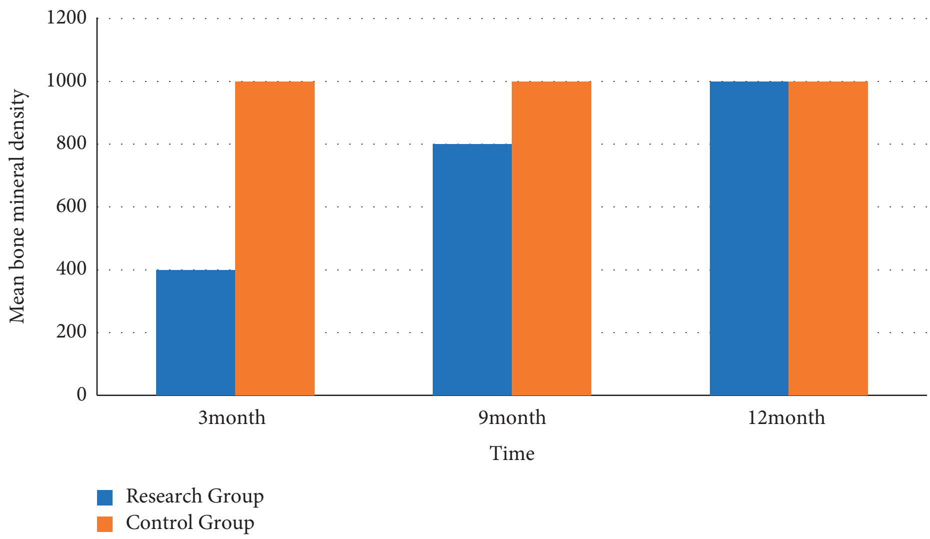

Figure 5: Changes in average bone density of teeth after root canal therapy under CBCT.

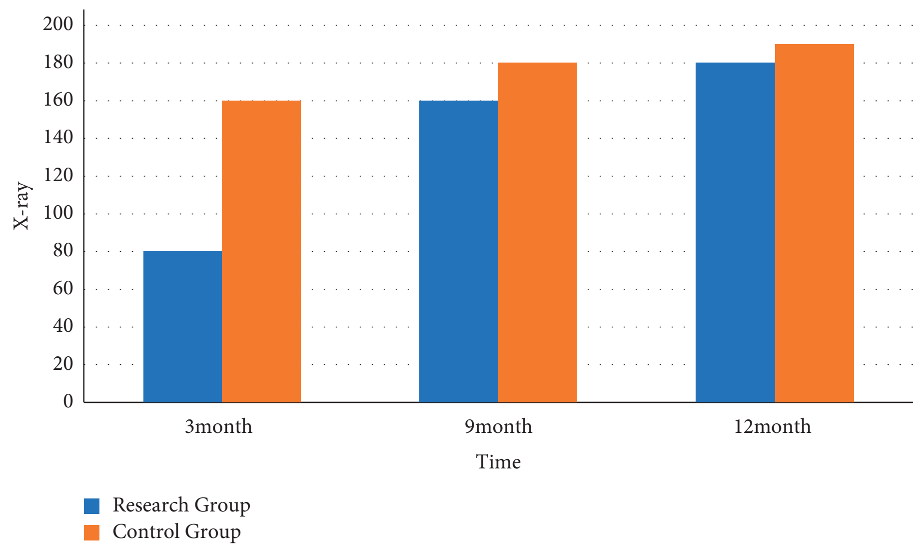

Figure 6: Changes in average bone density of teeth after root canal therapy under X-ray examination.

three key human diseases for prevention and treatment. The traditional imaging examinations for DPD are generally X-ray examinations and comprehensive tomographic examinations, but these examinations are all two-dimensional imaging examinations [15]. With the gradual increase in the precision requirements of modern medicine for imaging examinations, two-dimensional imaging examinations have gradually been unable to meet the requirements of dentists.

Compared with two-dimensional radiography, the relative advantages of three-dimensional radiography have promoted the use of CBCT. CBCT uses cone X-rays and area detectors for image acquisition because high-precision three-dimensional images can be obtained. Therefore, since the introduction of dentistry in 1998, CBCT has been increasingly used for orthodontic diagnosis, treatment planning, and research. The three-dimensional craniofacial and dental morphology of CBCT is very important to define the normal and abnormal three-dimensional anatomy of the structure, which may have long-term utility in diagnosis and treatment planning [16, 17]. According to relevant research results, CBCT will play a vital role in the following areas in the future: enhanced diagnosis, such as precise positioning of affected teeth and supernumerary teeth; quantifying the severity of craniofacial abnormalities and other defects and deformities; and improving the differential diagnosis of bone, dentistry, or combined breast, including identifying the jaw that causes breast rejection, and determining whether the difference is bilateral or unilateral, such as orthopedic surgery, asymmetry, craniofacial abnormalities, and open bite disease [18].

One of the main advantages of CBCT over two-dimensional radiography is that it can provide three-dimensional volume, surface, and partial information about the craniofacial structure. This allows orthodontists and researchers in this field to overcome the huge limitations of two-dimensional radiographs, including magnification,

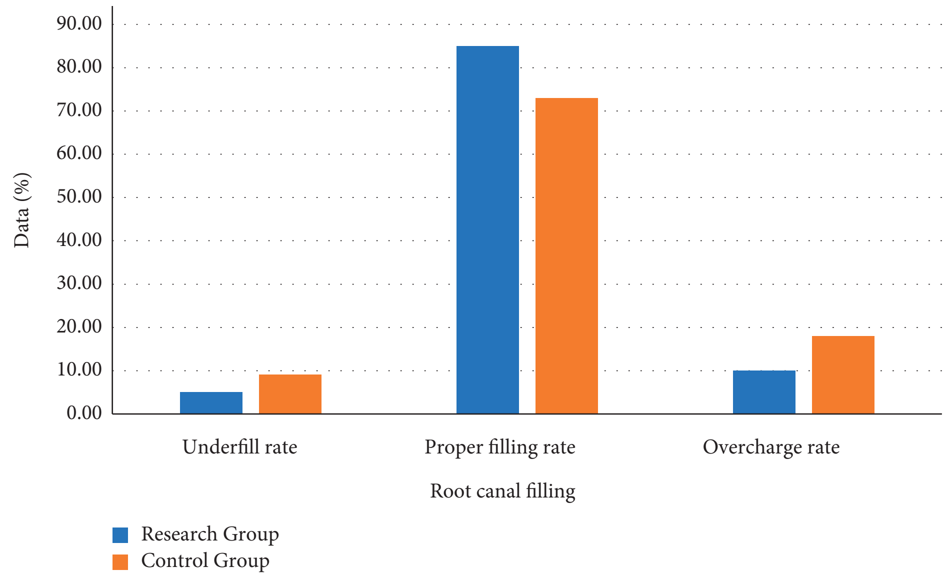

Figure 7: Comparison of the filling effect of root canal therapy in DPD.

geometric distortion, superimposed structures, and inconsistent head positions. In the early stages of merging CBCT for orthodontic purposes, there was a tendency to fold the three-dimensional data sets into three-dimensional images, because analyzing images in this way was the only known professional method to assess the relationship between dentistry and bone structure [19, 20]. Currently, CBCT can be used to analyze the three-dimensional craniofacial anatomy and treatment changes. CBCT can learn a lot from the two-dimensional caesarean section measurement method to obtain linear and angular measurements from three-dimensional images. However, extracting two-dimensional measurement results from three-dimensional images will cause the loss of key three-dimensional information and reduce the overall value of the three-dimensional data set. In addition, CBCT also uses shape correspondence, which determines the displacement of a given landmark between two time points, and represents these as vector and color-coded maps to depict the direction and amount of movement [21, 22]. In the future, similar methods may replace or supplement the linear and angular measurements produced by three-dimensional or planar reconstruction to process and analyze CBCT images.

5. Conclusion

In this study, the three-dimensional reconstruction algorithm was used to reconstruct the CBCT images of DPD patients, and on this basis, the diagnosis and root canal treatment of DPD patients were carried out. In addition, it was compared with the diagnosis and treatment effect under X-ray detection. It was found that the segmentation accuracy of the three-dimensional reconstruction algorithm for CBCT images was 84.7%, with an increase of 5.5%; the average UR was 5.3%, with a decrease of 5.7%; and the average OR was 3.1%, with an increase of 1.1%. Under the monitoring of the three-dimensional reconstruction of CBCT technology, the average bone density of the test group patients after 12 months of root canal treatment was the same as that of healthy people. In addition, the average bone density of the test group patients under X-ray detection was still lower than the average bone density of healthy people. Under the CBCT monitoring of three-dimensional reconstruction, the underfilling rate, proper filling rate, and overfilling rate of patients after root canal treatment were 5%, 85%, and 10%, respectively. This showed that CBCT technology based on intelligent three-dimensional reconstruction had a higher application prospect in DPD diagnosis and treatment. However, there were many limitations and deficiencies, such as a single imaging diagnosis method, insufficient sample size, and insufficient indicators for evaluating the efficacy of root canal therapy. In future studies, I would continue to study this topic in depth.

Data Availability

The data used to support the findings of this study are available from the corresponding author upon request.

Conflicts of Interest

The authors declare no conflicts of interest.

Acknowledgments

This work was supported by the Program for Young Talents of the Changzhou Commission of Health (QN202004) and Changzhou Sci&Tech Program (grant no: CJ20210092).

References

[1] C. Estrela, D. A. Decurcio, G. Rossi-Fedele, J. A. Silva, O. A. Guedes, and Á. H. Borges, "Root perforations: a review of diagnosis, prognosis and materials," *Brazilian Oral Research*, vol. 32, no. suppl 1, p. e73, 2018.

[2] M. Nakashima, K. Iohara, M. Murakami et al., “Pulp regeneration by transplantation of dental pulp stem cells in pulpitis: a pilot clinical study,” *Stem Cell Research & Therapy*, vol. 8, no. 1, p. 61, 2017.

[3] M. Nakashima and K. Iohara, “Recent progress in translation from bench to a pilot clinical study on total pulp regeneration,” *Journal of Endodontics*, vol. 43, no. 9S, pp. S82–S86, 2017.

[4] Q. Zhai, Z. Dong, W. Wang, B. Li, and Y. Jin, “Dental stem cell and dental tissue regeneration,” *Frontiers of Medicine*, vol. 13, no. 2, pp. 152–159, 2019.

[5] C. Morsczeck and T. E. Reichert, “Dental stem cells in tooth regeneration and repair in the future,” *Expert Opinion on Biological Therapy*, vol. 18, no. 2, pp. 187–196, 2018.

[6] C. Kichenbrand, E. Velot, P. Menu, and V. Moby, “Dental pulp stem cell-derived conditioned medium: an attractive alternative for regenerative therapy,” *Tissue Engineering Part B Reviews*, vol. 25, no. 1, pp. 78–88, 2019.

[7] Y. Itoh, J. I. Sasaki, M. Hashimoto, C. Katata, M. Hayashi, and S. Imazato, “Pulp regeneration by 3-dimensional dental pulp stem cell constructs,” *Journal of Dental Research*, vol. 97, no. 10, pp. 1137–1143, 2018.

[8] F. S. Schwindling, A. Tasaka, T. Hilgenfeld, P. Rammelsberg, and A. Zenthöfer, “Three-dimensional-guided removal and preparation of dental root posts-concept and feasibility,” *Journal of Prosthodontic Research*, vol. 64, no. 1, pp. 104–108, 2020.

[9] J. Meirinhos, J. N. R. Martins, B. Pereira et al., “Prevalence of apical periodontitis and its association with previous root canal treatment, root canal filling length and type of coronal restoration-a cross-sectional study,” *International Endodontic Journal*, vol. 53, no. 4, pp. 573–584, 2020.

[10] F. A. Restrepo-Restrepo, S. J. Cañas-Jiménez, R. D. Romero-Albarracín, P. A. Villa-Machado, M. I. Pérez-Cano, and S. I. Tobón-Arroyave, “Prognosis of root canal treatment in teeth with preoperative apical periodontitis: a study with cone-beam computed tomography and digital periapical radiography,” *International Endodontic Journal*, vol. 52, no. 11, pp. 1533–1546, 2019.

[11] A. A. Ozaslan, A. Alacaoglu, O. B. Demirel, T. Çukur, and E. U. Saritas, “Fully automated gridding reconstruction for non-Cartesian x-space magnetic particle imaging,” *Physics in Medicine and Biology*, vol. 64, no. 16, Article ID 165018, 2019.

[12] J. Meirinhos, J. Martins, B. Pereira, A. Baruwa, and A. Ginjeira, “Prevalence of lateral radiolucency, apical root resorption and periapical lesions in Portuguese patients: a CBCT cross-sectional study with a worldwide overview,” *European endodontic journal*, vol. 6, no. 1, pp. 56–71, 2021.

[13] A. Banerjee, J. E. Frencken, F. Schwendicke, and N. P. T. Innes, “Contemporary operative caries management: consensus recommendations on minimally invasive caries removal,” *British Dental Journal*, vol. 223, no. 3, pp. 215–222, 2017.

[14] F. Schwendicke, J. E. Frencken, L. Bjørndal et al., “Managing carious lesions,” *Advances in Dental Research*, vol. 28, no. 2, pp. 58–67, 2016.

[15] A. Farias Gomes, S. L. Sousa Melo, Y. Nejaim, F. C. Groppo, F. B. Teixeira, and D. Q. Freitas, “Variations in pulp volume between normotensive and hypertensive individuals on CBCT imaging,” *Clinical Oral Investigations*, vol. 24, no. 11, pp. 4069–4076, 2020.

[16] B. Pradhan, Y. Gao, L. He, and J. Li, “Non-surgical removal of dens invaginatus in maxillary lateral incisor using CBCT: two-year follow-up case report,” *Open Medicine*, vol. 14, no. 1, pp. 767–771, 2019.

[17] G. Meza, D. Urrejola, N. Saint Jean et al., “Personalized cell therapy for pulpitis using autologous dental pulp stem cells and leukocyte platelet-rich fibrin: a case report,” *Journal of Endodontics*, vol. 45, no. 2, pp. 144–149, 2019.

[18] T. Connert, M. S. Zehnder, M. Amato, R. Weiger, S. Kühl, and G. Krastl, “Microguided Endodontics: a method to achieve minimally invasive access cavity preparation and root canal location in mandibular incisors using a novel computer-guided technique,” *International Endodontic Journal*, vol. 51, no. 2, pp. 247–255, 2018.

[19] B. H. A. Mai, M. Drancourt, and G. Aboudharam, “Ancient dental pulp: masterpiece tissue for paleomicrobiology,” *Molecular genetics & genomic medicine*, vol. 8, no. 6, Article ID e1202, 2020.

[20] L. Hu, Z. Gao, J. Xu et al., “Decellularized swine dental pulp as a bioscaffold for pulp regeneration,” *BioMed Research International*, vol. 2017, pp. 1–9, Article ID 9342714, 2017.

[21] H. Maekawa, M. Nakao, K. Mineura, T. F. Chen-Yoshikawa, and T. Matsuda, “Model-based registration for pneumothorax deformation analysis using intraoperative cone-beam CT images,” *Annual International Conference of the IEEE Engineering in Medicine and Biology Society. IEEE Engineering in Medicine and Biology Society. Annual International Conference*, vol. 2020, pp. 5818–5821, 2020.

[22] X. Min, F. Lu, and C. Li, “Sequence-based deep learning frameworks on enhancer-promoter interactions prediction,” *Current Pharmaceutical Design*, vol. 27, no. 15, pp. 1847–1855, 2021.